BIOCHEMISTRY
including biophysical chemistry & molecular biology

Article

pubs.acs.org/biochemistry

Hybrid [FeFe]-Hydrogenases with Modified Active Sites Show Remarkable Residual Enzymatic Activity

Judith F. Siebel, Agnieszka Adamska-Venkatesh, Katharina Weber, Sigrun Rumpel, Edward Reijerse,* and Wolfgang Lubitz*

Max Planck Institute for Chemical Energy Conversion, Stiftstrasse 34-36, D-45470 Muelheim an der Ruhr, Germany

Supporting Information

ABSTRACT: [FeFe]-hydrogenases are to date the only enzymes for which it has been demonstrated that the native inorganic binuclear cofactor of the active site $Fe_2(adt)(CO)_3(CN)_2$ (adt = azadithiolate = $[S\text{-}CH_2\text{-}NH\text{-}CH_2\text{-}S]^{2-}$) can be synthesized on the laboratory bench and subsequently inserted into the unmaturated enzyme to yield fully functional holo-enzyme (Berggren, G. et al. (2013) *Nature 499*, 66−70; Esselborn, J. et al. (2013) *Nat. Chem. Biol. 9*, 607−610). In the current study, we exploit this procedure to introduce non-native cofactors into the enzyme. Mimics of the binuclear subcluster with a modified bridging dithiolate ligand (thiodithiolate, *N*-methylazadithiolate, dimethyl-azadithiolate) and three variants containing only one CN^- ligand were inserted into the active site of the enzyme. We investigated the activity of these variants for hydrogen oxidation as well as proton reduction and their structural accommodation within the active site was analyzed using Fourier transform infrared spectroscopy. Interestingly, the monocyanide variant with the azadithiolate bridge showed ∼50% of the native enzyme activity. This would suggest that the CN^- ligands are not essential for catalytic activity, but rather serve to anchor the binuclear subsite inside the protein pocket through hydrogen bonding. The inserted artificial cofactors with a propanedithiolate and an *N*-methylazadithiolate bridge as well as their monocyanide variants also showed residual activity. However, these activities were less than 1% of the native enzyme. Our findings indicate that even small changes in the dithiolate bridge of the binuclear subsite lead to a rather strong decrease of the catalytic activity. We conclude that both the Brønsted base function and the conformational flexibility of the native azadithiolate amine moiety are essential for the high catalytic activity of the native enzyme.

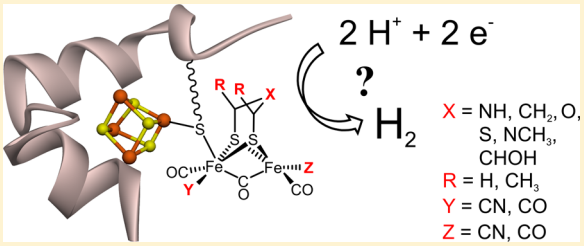

INTRODUCTION

Hydrogenases are enzymes that catalyze the reversible reaction of molecular hydrogen to electrons and protons: $H_2 \rightleftharpoons 2\ H^+ + 2\ e^-$.[1,2] Generally, the activation of hydrogen is difficult due to its strong, nonpolar H−H bond.[3] However, in hydrogenases, the reaction takes place at ambient temperature and pressure.[4−6] The two main classes of these enzymes are the [FeFe]-hydrogenases and [NiFe]-hydrogenases, named according to the metal ions present in their active sites.[7−10] In general, [FeFe]-hydrogenases are more active in H_2 production.[11] Understanding the function of these enzymes will form the basis for a rational design of efficient artificial systems for production of H_2 as a renewable energy carrier for the future.[12−18]

In [FeFe]-hydrogenases, the catalytic reaction takes place at the so-called H-cluster, a [4Fe-4S]-cluster connected via the thiolate of a cysteine residue to a binuclear [2Fe]-subsite[19] (Figure 1a,b). [FeFe]-hydrogenases from anaerobic bacteria bind several [FeS]-clusters in addition to the H-cluster,[7,8] whereas in the [FeFe]-hydrogenases of green algae like HydA1 from *Chlamydomonas reinhardtii*, these accessory [FeS]-cluster are absent.[6,20] In vivo, the [2Fe]-subsite is synthesized and inserted by the hydrogenase maturation proteins HydE, HydF, and HydG.[21,22] HydG has been recently shown to play a key role in the maturation process since it produces an $\{Fe(CO)_2(CN)\}$ "synthon" that can be regarded as the first precursor to the binuclear subsite.[23,24] The two Fe atoms of the [2Fe]-subsite are referred to as proximal (Fe_p) and distal (Fe_d) iron relative to the [4Fe-4S]-cluster and are connected via an azadithiolate bridge.[8] Each Fe is coordinated by a CO and CN^- ligand as well as an additional CO[25] which can be bridging or terminal depending on the redox state of the H-cluster.[26] Fe_p is six-coordinated, whereas Fe_d is five-coordinated leaving an open coordination site where H_2 production and oxidation are proposed to occur.[27−29] The unusual, small inorganic ligands CO and CN^- are strong field ligands that keep the Fe center in the low-spin state.[30]

Since the crystal structures of [FeFe]- and [NiFe]-hydrogenase were solved,[7−9,25,34,35] chemists started to synthesize model compounds that mimic their active sites.[1,15,16,18] In 1999, three groups separately reported the first [FeFe]-hydrogenase active site model $[Fe_2(pdt)(CO)_4(CN)_2]^{2-}$ **2a** (pdt = **p**ropane**di**thiolate, Figure 1c).[36−38] At that time, the nature of the bridgehead atom was not uniquely identified since

Received: November 7, 2014
Revised: January 22, 2015
Published: January 29, 2015

DOI: 10.1021/bi501391d
Biochemistry 2015, 54, 1474−1483

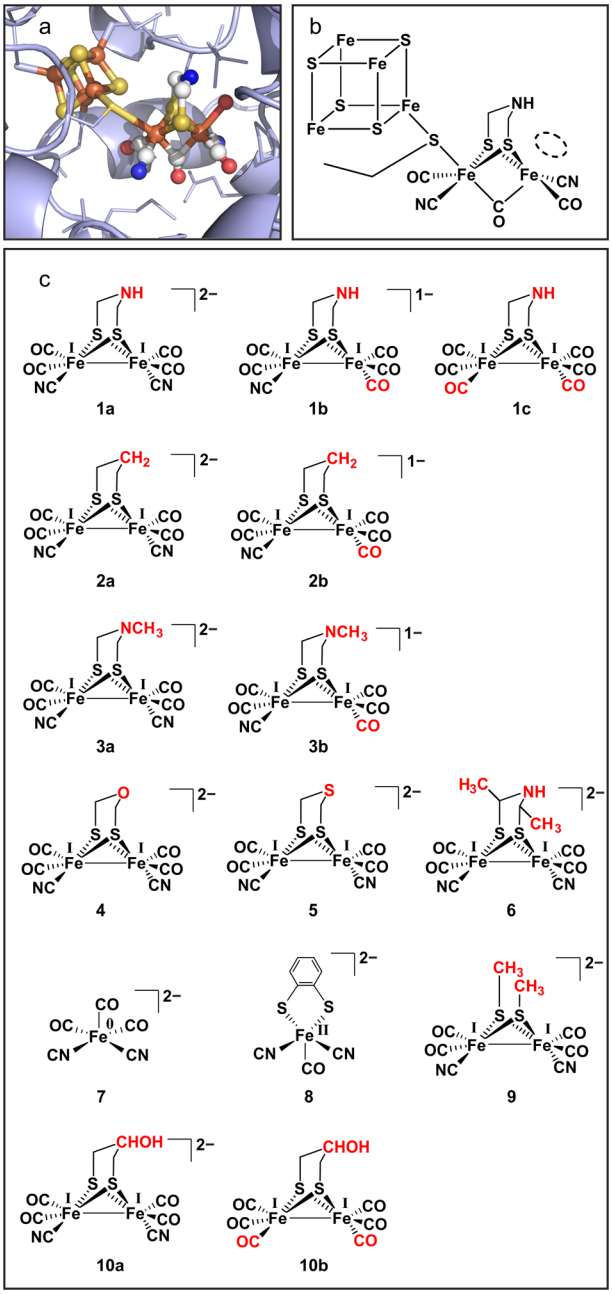

Figure 1. (a) Active site (H-cluster) of *C. reinhardtii* [FeFe]-hydrogenase HydA1 in its protein surrounding. The protein backbone is shown as well as the amino acid residues near the H-cluster. An alignment of the crystal structures of *C. reinhardtii* HydA1 (3LX4[31]) and *Clostridium pasteurianum* (3C8Y[32]) was used for the image, generated using the program PYMOL.[33] (b) Schematic structure of the H-cluster with the open coordination site shown as an ellipsoid. (c) Series of all [2Fe]-model compounds that were synthesized and used in the artificial maturation attempts of *C. reinhardtii* HydA1.

C, N, and O could not be distinguished at the available crystallographic resolution. Therefore, additional mimics $[Fe_2(adt)(CO)_4(CN)_2]^{2-}$ **1a** (adt = **a**za**d**i**t**hiolate) and $[Fe_2(odt)(CO)_4(CN)_2]^{2-}$ **4** (odt = **o**xa**d**i**t**hiolate) were synthesized[39,40] (see Figure 1c). As free complexes in solution **1a**, **2a**, and **4** have a low activity[1] and can therefore be classified as structural rather than functional active site models. A few years later, based on arguments related to the possible catalytic mechanism and a reanalysis of the crystal structure, Nicolet et al. proposed the nature of the bridgehead atom to be nitrogen.[19] This assignment was later experimentally supported by the magnetic resonance studies of Silakov et al.[41] and Erdem et al.[42]

Very recently, Berggren et al. demonstrated that **1a**, **2a**, and **4** can be bound to the native maturase HydF, which subsequently delivers the model compound to the unmaturated form of HydA1 that only contains the [4Fe-4S]-cluster but not the [2Fe]-subsite.[43] Since only the hybrid enzyme containing mimic **1a** showed full hydrogenase activity, this experiment provided unequivocal evidence for an amine function in the dithiolate bridging ligand.[43] Shortly thereafter, Esselborn et al. showed that **1a** can be inserted also directly into unmaturated HydA1[44] (i.e., unassisted by HydF). The hybrid HydA1-**1a** is fully active and indistinguishable from the native hydrogenase.[43,44] The electron paramagnetic resonance (EPR) and Fourier transform infrared (FTIR) spectra of HydA1-**1a** showed the same redox states as the native *Chlamydomonas reinhardtii* hydrogenase HydA1.[43−45] Subsequent FTIR spectroelectrochemical experiments revealed reduction potentials identical to those of the native enzyme.[45] The FTIR spectra of HydA1-bound **2a** and **4** exhibited vibrational modes from CO, bridging CO, and CN^- ligands similar to those of the native H-cluster, but no H_2 production activity was reported.[43]

In the current study, we investigate a series of model compounds that can be introduced into unmaturated HydA1 (Figure 1c). The central bridgehead atom was replaced by sulfur or the bulkier NCH_3 group (**5** and **3a**, respectively). Furthermore, the free volume of the protein pocket was probed by introducing methyl groups on the adt methylene moieties (**6**). Finally, three variants with only one CN^- ligand were synthesized in order to explore the function of the CN^- ligands (**1b**, **2b**, and **3b**). The successful insertion of these variants was monitored by FTIR spectroscopy and the new hybrid proteins were tested for their residual H_2 production and oxidation activity using gas chromatography and UV spectroscopy, respectively. None of these variants showed improved hydrogenase activity. Nevertheless, very interesting insight into the conformational and functional features of the active site could be gained by studying the properties of these hybrid hydrogenases.

MATERIALS AND METHODS

Preparation of Unmaturated HydA1. The structural gene of *C. reinhardtii* HydA1 was heterologously overexpressed in *E. coli* BL21(DE3)Δ*iscR*[46] according to a procedure previously described by Kuchenreuther et al.[47] but without expression of the maturases HydE, HydF, HydX, and HydG. For overexpression, a pET21b expression plasmid containing an *E. coli* codon optimized *C. reinhardtii* HydA1 gene with an N-terminal Strep-tag followed by a TEV (tobacco etch virus) cleavage site (WSHPQFEKSSGRENLYFQ|G) was used. After purification on a Strep-Tactin Superflow high capacity resin (IBA GmbH), TEV protease was added to unmaturated HydA1 at a ratio of 1:30 (w/w) and incubated overnight at room temperature to cleave the Strep-Tag. The plasmid for expression of the TEV protease was a gift from the Arrowsmith laboratory (University of Toronto). The His_6-tagged TEV protease was removed by addition of Talon metal affinity resin (Clontech, 350 μL column volume Talon beads per mg TEV), incubation for 1 h, and separation of the beads from the protein solution by filtration. Successful TEV-cleavage was confirmed by mass spectrometry (Supporting Information Figure S1a).

DOI: 10.1021/bi501391d
Biochemistry 2015, 54, 1474−1483

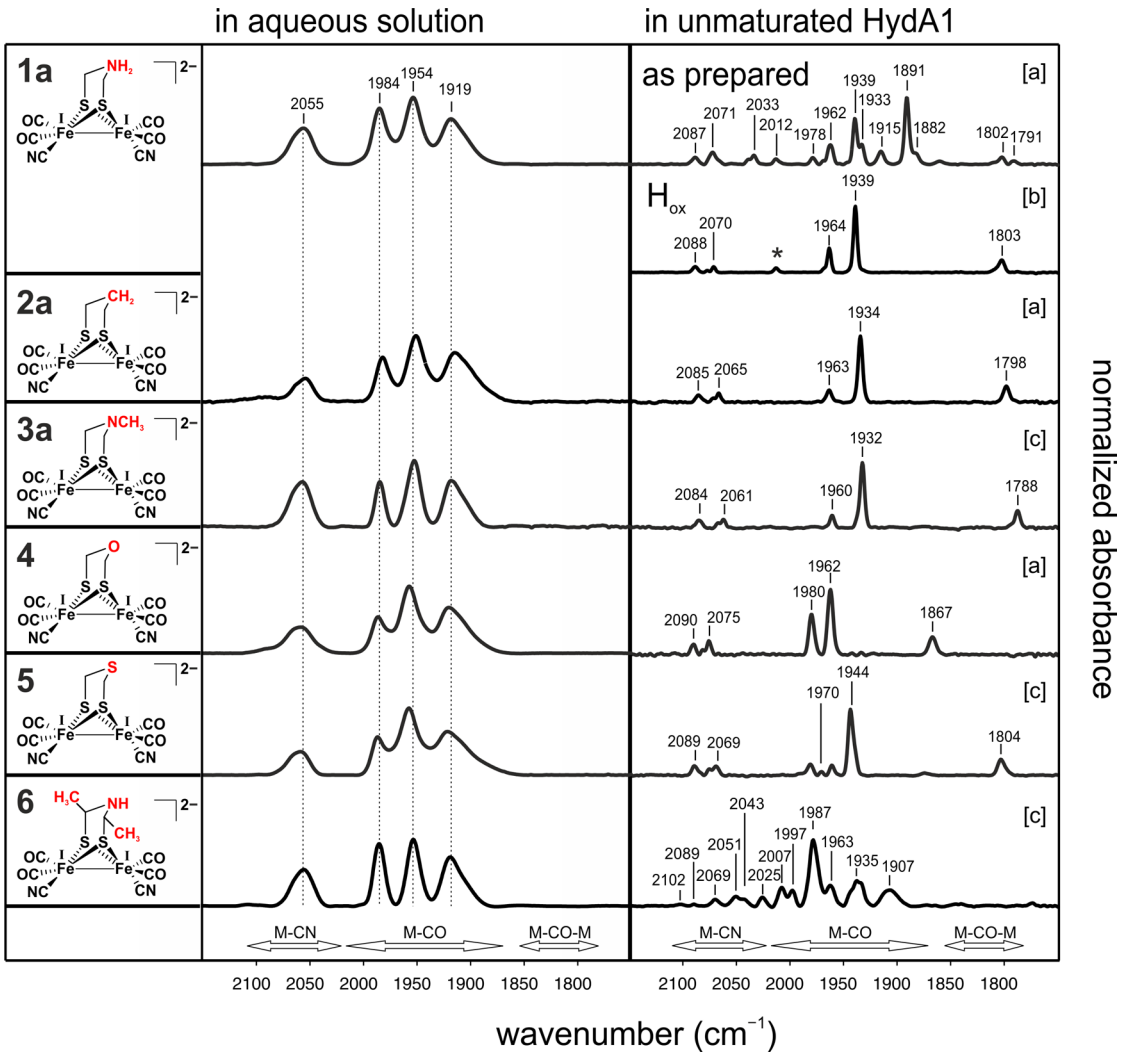

Figure 2. Synthetic complexes **1a**, **2a**, **3a**, **4**, **5**, and **6** (left) and FTIR spectra of those as free complex (middle) and inserted into unmaturated HydA1 (right) as indicated. HydA1-**1a** is shown as-prepared and in the H_{ox}-state. Spectra were measured at 15 °C in 25 mM Tris/HCl, pH 8.0, 25 mM KCl (and 2 mM NaDT in HydA1-**x**). [a] Ref 43. [b] Ref 45. [c] This work. * peak of CO-inhibited state.

Protein samples (Supporting Information Figure S1b, S1c) were concentrated to 0.5−4 mM in 100 mM Tris/HCl, pH 8.0, 150 mM NaCl, 2.5 mM desthiobiotin, and 2 mM NaDT (sodium dithionite), sealed anaerobically, and stored at −80 °C until use.

Reconstitution with Synthetic Active Site Mimics. All samples were handled under strict anaerobic conditions. For FTIR samples, a concentrated solution of unmaturated HydA1 prepared as described above was diluted in dilution buffer (25 mM Tris/HCl, pH 8.0, 25 mM KCl, and 2 mM NaDT) to reach a concentration of 50−150 μM. Fivefold excess of either $[Fe_2(xdt)(CO)_4(CN)_2]^{2-}$ (xdt refers to one of the dithiolate bridge variants) or $[Fe_2(xdt)(CO)_5(CN)]^-$, dissolved in DMSO, was added and the mixture was incubated for 1 h at room temperature. Excess of free synthetic complex was removed using PD-10 desalting columns (GE Healthcare). For $[Fe_2(adt)(CO)_5(CN)]^-$ the procedure was slightly different: it was dissolved in acetonitrile, the dilution buffer contained 10 mM NaDT, and protein samples were additionally desalted on a PD-10 column using the dilution buffer supplemented with 10% acetonitrile in order to remove unspecifically bound complex. After desalting, the protein samples were concentrated to 0.5−4 mM and used immediately or stored at −80 °C until use.

For activity measurements, a concentrated solution of unmaturated HydA1 was diluted to 1.5−40 μM. A 10-fold excess of synthetic complex was added and the mixture was incubated for 1 h at room temperature. The samples were used immediately for activity tests. For HydA1-**1b**, the maturation process was performed in the presence of 10 mM NaDT.

FTIR Analysis. FTIR spectra of $[Fe_2(xdt)(CO)_4(CN)_2]^{2-}$ and unmaturated HydA1 maturated with any of the synthetic mimic variants (referred to as HydA1-**x** here) were measured in 25 mM Tris/HCl, pH 8.0, 25 mM KCl, and dilution buffer, respectively. Spectra of $[Fe_2(xdt)(CO)_5(CN)]^-$ were measured in DMSO. All spectra were obtained on a Bruker IFS 66v/s FTIR spectrometer equipped with a Bruker nitrogen cooled MCT (mercury cadmium telluride) detector. The spectra were accumulated in the double-sided, forward−backward mode with 100−1000 scans and a resolution of 2 cm^{-1} at 15 °C. Data processing was facilitated by home-written routines in the MATLAB programming environment.

Hydrogen Production Assay. Hydrogen production was determined according to the procedure described by Winkler et al.:[48] the amount of HydA1-**x** (1−20 μL) corresponding to

DOI: 10.1021/bi501391d
Biochemistry 2015, 54, 1474−1483

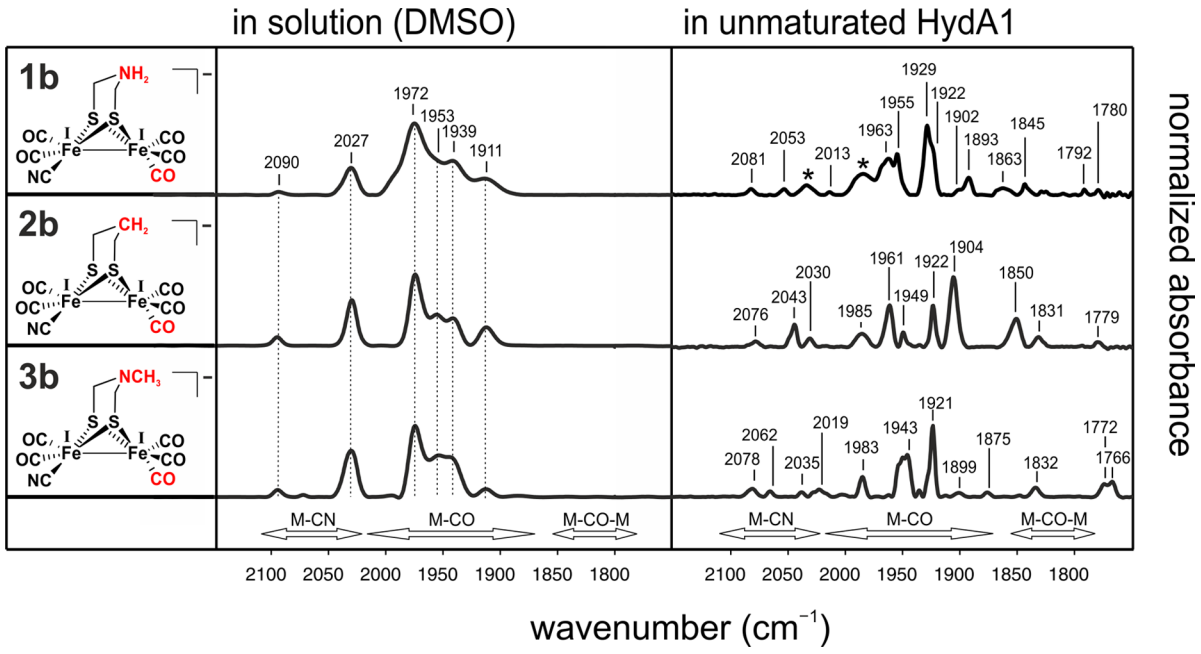

Figure 3. Synthetic complexes **1b**, **2b**, and **3b** (left) and FTIR spectra of those as free complex (middle) and in unmaturated HydA1-bound form (right) as indicated. Spectra of HydA1-**x** were measured at 15 °C in 25 mM Tris/HCl, pH 8.0, 25 mM KCl, 2 or 10 mM NaDT. The free complexes were measured in DMSO. *peak of the free complex **1b**.

100 ng (HydA1-**1a** and HydA1-**1b**) or 10 μg (all others) was added to a total amount of 400 μL 100 mM potassium phosphate, pH 6.8, 100 mM NaDT, and 10 mM methyl viologen in a 2 mL vial sealed under anaerobic conditions (Suba-seal septa, 13, Sigma-Aldrich). After flushing with argon for 5 min and incubation at 37 °C for 20 min, a gas chromatogram was recorded on a 6890 Series GC System (Agilent Technologies) using a molecular sieve 5 Å PLOT column by injecting 300 μL of the headspace gas.

Hydrogen Oxidation Assay. Hydrogen oxidation was measured anaerobically as previously described[47] with the following modifications: the amount of HydA1-**x** (1−20 μL) prepared corresponding to 100 ng (HydA1-**1a** and HydA1-**1b**) or 10 μg (all others) was added to 1 mL 100 mM potassium phosphate, pH 6.8, 10 mM methyl viologen and spectrophotometrically analyzed at 25 °C for 3−30 min depending on the activity (using an Ocean Optics USB2000+XR1-ES, equipped with a DH-MINI Deuterium Tungsten Halogen Source).

Iron Quantification. For iron quantification (see Supporting Information, notes on activity measurements), the samples were prepared as described for FTIR (see above) and used immediately. For each sample, the iron content was determined three times for three different protein concentrations according to the literature procedure.[49]

Synthesis. All reactions were carried out under an inert atmosphere of argon using standard Schlenk-techniques or in a dry argon glovebox (MBraun LabMaster130). Acetonitrile, dichloromethane, diethyl ether, and *n*-hexane were purified by the solvent purification system MBraun MB SPS-800 Auto. THF used was dried over sodium with benzophenone and distilled under argon. The compounds presented in Figure 1c were synthesized corresponding to literature procedures. The dicyanide compounds $[Fe_2(xdt)(CO)_4(CN)_2]^{2-}$ and $[Fe_2(SCH_3)_2(CO)_4(CN)_2]^{2-}$ were synthesized from the corresponding hexacarbonyl compounds $[Fe_2(xdt)(CO)_6]$ (xdt = adt,[39] pdt,[37,50] odt,[39,40] dime-adt,[51] NMedt,[39] tdt,[52] OHpdt[53]), and $[Fe_2(SCH_3)_2(CO)_6]$[54] using a standard procedure described in the Supporting Information.[37,38] Monosubstituted derivatives of the type $[Fe_2(xdt)(CO)_5(CN)]^-$ were obtained using the decarbonylation agent Me_3NO followed by addition of $[NEt_4][CN]$[55] (see Supporting Information). The synthesis of **7** and **8** was carried out as reported previously.[56,57]

RESULTS

Insertion of the Dicyanide Compounds with Different Bridgehead Groups. The CN and CO stretch vibrations as observed in FTIR spectroscopy are very sensitive to changes in the oxidation states of the [2Fe]-core in the H-cluster. Moreover, slight changes in hydrogen bonding and electrostatic interactions with the surrounding protein pocket are reflected in the FTIR spectra as well. In this work, FTIR was used to check if the complexes are incorporated into unmaturated HydA1 as reported previously for $[Fe_2(adt)(CO)_4(CN)_2]^{2-}$ **1a**, $[Fe_2(pdt)(CO)_4(CN)_2]^{2-}$ **2a**, and $[Fe_2(odt)(CO)_4(CN)_2]^{2-}$ **4**.[43] We synthesized three additional complexes with variations in the dithiolate bridge: $[Fe_2(NMedt)(CO)_4(CN)_2]^{2-}$ **3a** (NMedt = ***N*-Me**thylaza**di**thiolate), an *N*-methyl analogue of adt,[39] $[Fe_2(tdt)(CO)_4(CN)_2]^{2-}$ **5** (tdt = **t**hio**di**thiolate) with a sulfur atom in the bridgehead,[52] and $[Fe_2(dime\text{-}adt)(CO)_4(CN)_2]^{2-}$ **6** (dime-adt = **dime**thyl-aza**di**thiolate) with two methyl groups in the azadithiolate backbone[51] (Figure 1c).

Figure 2 (middle) shows the FTIR spectra of the free model compounds **1a**, **2a**, **3a**, **4**, **5**, and **6**. All six spectra are very similar showing broad bands due to geometrical flexibility of the molecules in solution. The corresponding stretching modes are assigned on the basis of DFT (density functional theory) calculations and are listed in the Supporting Information (Figure S3). The overall pattern is in agreement with previously reported data.[55] Upon binding to unmaturated HydA1, the respective complex is immobilized in the protein leading to a sharpening of the FTIR bands. This was observed for all

DOI: 10.1021/bi501391d
Biochemistry 2015, 54, 1474−1483

complexes and is indicative of successful insertion (Figure 2, right[43,45]). It is remarkable that methylation of the bridging amine leading to $[Fe_2(NMedt)(CO)_4(CN)_2]^{2-}$ **3a** does not impair insertion of the mimic complex. On the other hand, the substantially increased steric demand of $[Fe_2(dime\text{-}adt)(CO)_4(CN)_2]^{2-}$ **6** results in a slight broadening of the FTIR bands as compared to other complexes. The complicated FTIR spectrum suggests the occurrence of multiple species or conformations of the mimic complex which are not properly immobilized inside the protein pocket. The variants HydA1-**2a**, -**3a**, -**4**, and -**5** show a simple five peak pattern consistent with one single redox (and conformational) state. The peak patterns of HydA1-**2a**, -**3a**, and -**5** strongly resemble that of H_{ox}[43] (for the assignment of the corresponding stretching modes of H_{ox}, see Supporting Information Figure S4). The FTIR spectrum of HydA1-**4** clearly deviates from that of H_{ox} but still reveals an H-cluster-like signature showing the characteristic stretching modes of H_{ox} (Supporting Information Figure S4).

Insertion of the Monocyanide Compounds with Different Bridgehead Groups. To test whether both CN^- ligands of the [2Fe]-subsite are required for binding to unmaturated HydA1, we synthesized variants of **1a**, **2a**, and **3a** where only one CO ligand is replaced by a CN^- ligand instead of two in the last synthesis step,[55] namely, $[Fe_2(adt)(CO)_5(CN)]^-$ **1b**, $[Fe_2(pdt)(CO)_5(CN)]^-$ **2b**, and $[Fe_2(NMedt)(CO)_5(CN)]^-$ **3b** (Figure 1c). The FTIR spectra of the monocyanide variants in solution (Figure 3, middle) are in agreement with reported data[55] and the corresponding stretching modes are shown in Supporting Information Figure S5. As verified by FTIR spectroscopy, **1b**, **2b**, and **3b** can all be inserted into unmaturated HydA1, clearly showing that one CN^- is sufficient for HydA1-binding (Figure 3, right). Surprisingly, **1b** showed some unspecific binding of the complex to unmaturated HydA1. Most of the unspecifically bound complex could be removed by using desalting buffer containing 10% organic solvent (acetonitrile). Nevertheless, some features of the free complex can be seen in the spectrum (Figure 3, right top). The spectra for all HydA1 monocyanide variants are more complex than those for HydA1-**2a**, -**3a**, -**4**, and -**5**, suggesting the occurrence of multiple redox states and/or conformations. As will be discussed below, the increased structural complexity of the monocyanide H-cluster variants is most likely due to the fact that their precursor complexes are already asymmetric prior to insertion.

Insertion of Mononuclear Iron, All-Carbonyl, and Additional Dicyanide Compounds. Apart from the synthetic compounds already described, several others (Figure 1c) including mononuclear iron and all-carbonyl compounds were incubated with unmaturated HydA1. Except for $[Fe(CN)_2(CO)_3]^{2-}$ **7**, insertion was unsuccessful. The most common problem is insolubility and instability in water which turned out to be the case for **8**, **1c**, **9**, and **10b** (see Supporting Information). Complex **10a** $[Fe_2(OHpdt)(CO)_4(CN)_2]^{2-}$ (OHpdt = hydroxo-**p**ropane**di**thiolate) is more polar than **1a**, **2a**, **3a**, **4**, **5**, and **6** and fully soluble in aqueous solution. Nevertheless, insertion into unmaturated HydA1 could not be confirmed using FTIR spectroscopy. After incubation of the mononuclear iron compound **7** and unmaturated HydA1, various peaks could be detected in the FTIR spectrum, indicating successful incorporation (see Supporting Information Figure S6). Based on the complex spectrum, we assume that **7** has multiple binding modes inside the protein.

H_2 Production and Oxidation Activities. The activities of HydA1-**x** were determined for both H_2 production and oxidation. The activity values were obtained using identical maturation conditions (except for a slightly different buffer in the case of **1b**), but were not corrected for the degree of maturation, i.e., the amount of protein containing the corresponding synthetic mimic (for further details see Supporting Information Figure S2). HydA1-**1a** and HydA1-**1b** showed high activity (Figure 4). Also, activities for the much

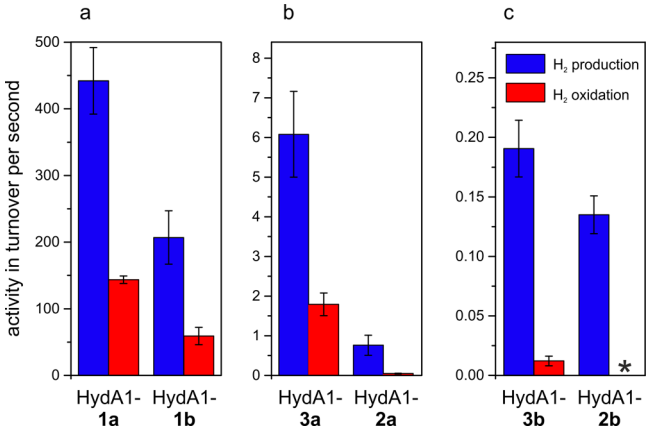

Figure 4. HydA1-**x** activities given in turnover frequencies (TOF) for H_2 production (blue bars) and oxidation (red bars) under identical maturation conditions. The activity tests were carried out in 100 mM potassium phosphate, pH 6.8, 10 mM methyl viologen with the addition of 100 mM NaDT in the case of H_2 production. It should be noted that the *y*-axis is different in a–c. Table S1 in the Supporting Information lists all activity values. (a) Activities of HydA1-**1a** and HydA1-**1b**. (b) Activities of HydA1-**3a** and HydA1-**2a**. (c) Activities of HydA1-**3b** and HydA1-**2b**. All samples were measured at least as triplicate from one preparation. For more details see the Supporting Information. *at detection limit.

less active hybrids HydA1-**2a** and HydA1-**3a** were observed. HydA1-**2b** and HydA1-**3b** showed some residual activity. The H_2 oxidation activity of HydA1-**2b** is at the detection limit of 0.003 s^{-1}. Activities for HydA1-**4**, HydA1-**5**, and HydA1-**6** could not be detected. It is remarkable that the HydA1 monocyanide variants consistently show a fraction of the activity of their HydA1 dicyanide parent complexes. Furthermore, both H_2 production and oxidation of the active HydA1-**x** hybrids are affected in the same way. This suggests that the enzymatic reaction in both directions relies on the same physical properties of the [2Fe]-subsite. All activity values can be found in the Supporting Information (Table S1).

DISCUSSION

The unassisted insertion of the binuclear subsite precursors into the unmaturated HydA1 protein is a remarkable feat of nature which is not yet fully understood. It is assumed that the protein contains an access channel that directs the precursor toward the active site pocket. In the unmaturated structure of *C. reinhardtii* HydA1 this channel is visible.[31] It is lined with hydrophilic side-chains that would allow insertion of the water solvated precursor through an entropically driven process.[58] Once arrived at its destination, the [2Fe]-precursor must form a covalent bond with the thiolate group of Cys_{225} which coordinates the cubane subcluster. In addition, the precursor must change its coordination sphere and adopt the "rotated

DOI: 10.1021/bi501391d
Biochemistry 2015, 54, 1474–1483

conformation" at the distal iron to accommodate an open coordination site. During this process, also the supernumerary CO ligand must dissociate.[44] It is likely that the hydrogen bond of the distal CN^- ligand to Lys_{228} that is embedded in a strong salt bridge network,[59] plays a key role in this conformational rearrangement. Apart from the covalent thiolate bridge with Cys_{225}, the binuclear part of the H-cluster is only held in position by electrostatic forces and hydrogen bonds via the CN^- ligands[60] (see Figure 5). One can therefore anticipate that

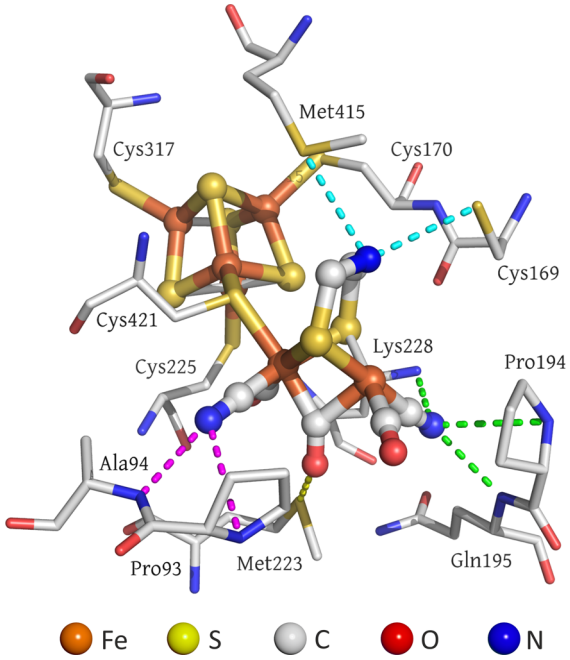

Figure 5. H-cluster in *C. reinhardtii* HydA1 with its protein surrounding. Interactions of the proximal CN^- ligand with the protein backbone are shown in pink and of the distal CN^- in green. Interactions of the bridging nitrogen with the protein surrounding are depicted in cyan. The interaction of the bridging CO with Met_{223} is shown in yellow. The picture is designed on the basis of the crystal structure of *Cp*I[32] using the program PYMOL.[33]

slight changes in the binuclear subcluster ligand sphere as well as the bridgehead group will have a strong effect on the insertion mechanism and the catalytic activity. The series of 15 model complexes (Figure 1c) that are presented in this study cover a wide range of size, charge, polarity, and bridgehead properties that can be used to probe the insertion channel and the protein surrounding of the H-cluster.

Insertion Channel and H-Cluster Protein Pocket. The H-cluster is located in a cavity inside the HydA1 protein. From there, a hydrophilic channel, 8−15 Å wide and about 25 Å deep, leads to the protein surface.[31] The mononuclear iron compound **7** is significantly smaller than the native [2Fe]-subsite. It can easily pass through the channel and bind to the active site cavity since it has been shown to be inserted into unmaturated HydA1 by FTIR spectroscopy (Supporting Information Figure S6). The spectrum features numerous peaks in the region of CN, CO, and bridging CO, indicating the presence of different states. Compound **7** is small relative to the space provided in the protein pocket and might be able to adopt different orientations since it is not fixed in a certain position like the native [2Fe]-subsite.

In order to find out if the channel and the cavity provide space for a [2Fe]-subsite larger than the native one, we synthesized two [2Fe]-subsite compounds **3a** and **6**, which have additional steric bulk. **3a** has a methyl group on the bridgehead nitrogen, and in **6**, two methylene protons are replaced by methyl groups (Figure 1c). The additional methyl groups do not prevent insertion into unmaturated HydA1, clearly showing that the compounds **3a** and **6** can pass the channel and bind in the active site cavity. It can be concluded that the H-cluster protein pocket provides more space than needed for the native [2Fe]-subsite. Complex **6** is the bulkiest synthetic compound inserted into HydA1 so far and might be close to the limit in size that we can include in the H-cluster protein pocket. Compound **10a**, with its hydroxo-propane-dithiolate bridge, is sterically less demanding than **3a** and **6**. However, insertion into unmaturated HydA1 could not be detected. Compound **10a** is fully soluble in water as it is more polar than all other compounds discussed in this work. This high polarity might be connected to its unsuccessful insertion. Possibly, the solvation shell is too tightly bound to **10a** and cannot be stripped off upon the attempt to enter the channel. Hence, it is too big to pass through the channel and no insertion can occur.

Interactions between the H-Cluster and the Protein Pocket. As already described, the [2Fe]-subsite of the H-cluster forms a covalent bond with a cysteine sulfur which connects it to the [4Fe-4S]-cluster. Apart from that, the strongest interactions of the [2Fe]-subsite with the protein surrounding are H-bonds and other electrostatic interactions (Figure 5).[60] In order to explore which interactions are necessary for binding, some of the hybrids synthesized lack specific interactions of the [2Fe]-subsite to the nearby amino acids. For example, in HydA1-**2a**, no H-bond between Cys_{169} and the bridgehead is possible. Also the electrostatic interactions between Met_{415} and the bridgehead are missing. Despite this, **2a** can be inserted into unmaturated HydA1. HydA1-**2b** carries a CO ligand instead of the second CN^- ligand. Therefore, there are two different orientations of the [2Fe]-subsite possible with respect to the [4Fe-4S]-cluster. In principle, both orientations can be obtained;[58] however, the orientation with the distal CN^- might be favored due to a strong H-bond to the side chain of Lys_{228}.[41,61] In any case, the interaction of the protein surrounding with one of the CN^- ligands is absent. Certainly, this does not prevent binding to unmaturated HydA1. It is therefore apparent that the interactions between nearby amino acids and the CN^- ligands are not crucial for the insertion process itself, but they might be important for subsequent stabilization of the [2Fe]-subsite inside the protein pocket.

Structural Effects of the Bridgehead Group. The native binuclear [2Fe]-subsite has an NH group in the bridging dithiolate ligand. In this study, the bridges modified with CH_2, O, S, or NCH_3 are exploited. The FTIR spectra do not differ much depending on the bridgehead (Figure 2, right), matching the results of DFT calculations by Yu et al.[62] HydA1-**2a**, -**3a**, and -**5** have a very similar pattern resembling HydA1-**1a**-H_{ox}. This indicates that all compounds are similarly bound to unmaturated HydA1 in a "rotated conformation" and that the supernumerary CO is dissociated. Presumably, the [2Fe]-subsite is in the redox state Fe^IFe^{II} as suggested for HydA1-**2a** based on EPR measurements.[45] Interestingly, the IR frequencies of all peaks of HydA1-**4** are shifted to higher energies. This is particularly pronounced for the bridging CO at

DOI: 10.1021/bi501391d
Biochemistry 2015, 54, 1474−1483

1867 cm^{-1}, indicating that the CO has significantly reduced bridging character. However, it is not a terminal ligand on one iron since its frequency is clearly distinct from that of the other CO groups. A shift to higher wavenumber compared to H_{ox} is also observed for the inactive state H_{inact} or H_{trans} of *Desulfuvibrio desulfuricans*[30,63] (see Supporting Information Table S2), where the distal iron carries an additional ligand which was postulated to be a hydroxo group.[7] Such a ligand might be stabilized by the oxygen bridgehead. Ligand binding to the open coordination site (H_2, H_2O) or protonation of the bridgehead oxygen in HydA1-**4** seems rather unlikely based on calculations[62] (see also Supporting Information Table S2). We suggest that although the central bridgehead atoms in HydA1-**4** (O) and HydA1-**5** (S) are isosteric and isoelectronic, it is their interaction with the protein surrounding that gives rise to differences in the spectra. However, HydA1-**5** has an additional component in the spectrum (Supporting Information Figure S7), probably indicating a second, minor species that has a similar structure to HydA1-**4**.

Structural Effects of the Ligand Sphere. HydA1-**1b**, HydA1-**2b**, and HydA1-**3b** contain a CO ligand instead of the second CN^- ligand found in HydA1-**1a**, -**2a**, and -**3a**. The FTIR spectra of HydA1-**2b** and HydA1-**3b** are more complex than those for HydA1-**2a** and -**3a** (Figures 2 and 3). For all HydA1 monocyanide variants, the two different orientations of the [2Fe]-subsite with respect to the [4Fe-4S]-cluster might contribute to the complexity of the spectra. Also, this increased structural complexity of the monocyanide H-cluster variants is likely related to the asymmetric nature of their precursor complexes prior to insertion. The FTIR spectrum of HydA1-**1b** is also complex but may additionally be explained by the occurrence of a mixture of different catalytically active states. Based on DFT calculations, it seems likely that the spectra of HydA1-**2b** and HydA1-**3b** contain signals from the [2Fe]-subsite in the oxidation states Fe^IFe^{II} and Fe^IFe^I (Supporting Information Figure S8, Table S3, Figure S9).

HydA1-**6** has modifications in the second ligand sphere: the two methylene groups of the dithiolate ligand are modified by one CH_3 group each instead of a proton. This leads to a FTIR spectrum that features various peaks (Figure 2, right bottom). They arise from a mixture of different isoforms and oxidation states (see Supporting Information Figure S10). Changes in the ligand sphere have a strong structural effect on the [2Fe]-subsite as can be seen from the FTIR spectra.

Catalytic Mechanism and Proton Transfer. In the catalytic cycle, H_2 is reversibly and heterolytically split into protons and electrons. The distal iron of the [2Fe]-subsite functions as an electron buffer and the protons presumably bind to the bridgehead nitrogen and are transported from there to the surface.[64] Our experiments revealed, however, that HydA1-**2a** with a CH_2 group in the bridgehead has some remaining activity, which is decreased by 3 orders of magnitude as compared to HydA1-**1a** (Figure 4). The catalytic cycle must therefore work differently from that of HydA1-**1a**, since no protonation of the methylene bridge can occur. More than a decade ago, the bridgehead was suggested to be CH_2.[7,8] Therefore, several mechanisms were proposed that did not include protonation of the bridgehead atom.[65−67] It was instead assumed that one of the sulfurs of the dithiolate bridge is protonated. Basically, one of those functional but, apparently, less efficient mechanisms could occur in HydA1-**2a**. Also for these mechanisms redox activity of the H-cluster is required. Recently we reported a detailed spectroscopic investigation of HydA1-**2a**, where, indeed, two different redox states with a one-electron-oxidation transition were identified.[45] The low activity of HydA1-**2a** is probably connected to the lower basicity of the bridging dithiolate group as well as their unfavorable positioning with respect to the proton channel of the enzyme. Supposedly, Cys_{169} is the first amino acid of this chain that is within H-bonding distance of the amine bridge[60,64] (Figure 5). Clearly, the distance of Cys_{169} to the bridging dithiolates is larger, which considerably slows down proton transfer. For efficient catalysis, it seems, therefore, important that a proton transfer chain is close to the first proton acceptor of the active site.

Following the pendant base paradigm, a decreased activity going from a polar bridgehead (HydA1-**1a**) to a less polar (HydA1-**4** and HydA1-**5**) and eventually to a nonpolar bridgehead (HydA1-**2a**) is expected. Experimentally, however, we find that only the nonpolar variant HydA1-**2a** has residual activity. Apparently, the catalytic mechanism of HydA1-**1a** depends not only on the correct positioning of the amine group with respect to the proton channel, but also on additional H-bonding and electrostatic interactions of the amine group with residues Cys_{169} and Met_{415}. Supposedly, these interactions are disturbed for HydA1-**4** and HydA1-**5** resulting in a collapse of the main catalytic mechanism. The question then arises why the mechanism proposed for HydA1-**2a** does not work for HydA1-**4** and HydA1-**5**. The most likely explanation is the stronger basicity of the dithiolate sulfurs in HydA1-**2a** than in HydA1-**4** and HydA1-**5** because of the positive inductive effect of the additional methylene group. This increases the electron density on the thiolate sulfur atoms and favors protonation compared to HydA1-**4** and HydA1-**5**.

HydA1-**3a** and -**6** both have a nitrogen atom in the bridgehead. Its basicity should be approximately the same as for HydA1-**1a**, because it was shown to be the same within error for the free complexes $[Fe_2(adt)(CO)_6]$, $[Fe_2(NMedt)(CO)_6]$, and $[Fe_2(dime\text{-}adt)(CO)_6]$.[51] Nevertheless, the activity of HydA1-**3a** is decreased and HydA1-**6** is inactive. The reason might be that the steric demand of the methyl groups impedes protonation or disturbs the fine-tuned fit in the protein pocket leading to no or lower activity. It is also possible that the protein surrounding changes the basicity of the nitrogen in HydA1-**1a**, -**3a**, and -**6** in a different way. In HydA1-**3a**, the methyl group on the nitrogen can be oriented either toward Cys_{170} (equatorial) or toward the open cavity (axial) (Figure 5). The axial position of the methyl group is probably sterically favored. However, in this conformation the lone pair of the bridgehead nitrogen is not accessible for the proton which arises from H_2 splitting at the distal iron site. HydA1-**3a** is the hybrid with the third highest activity of all semisynthetic hydrogenases, emphasizing the importance of the amine in the bridgehead (see previous section). In contrast, in HydA1-**6**, the steric bulk of the additional methyl groups and/or the complex stereochemistry eliminate all catalytic ability.

HydA1-1b. Of all the semisynthetic hydrogenases presented here, only HydA1-**1b** shows activity that is close to the native HydA1 and the hybrid HydA1-**1a**. Regarding the different key properties identified as crucial for a functional hydrogenase, most of these are given for HydA1-**1b**: The bridgehead atom is the same as in the native system, the protein pocket has the appropriate size for the synthetic [2Fe]-subsite, and the proton formed upon H_2 splitting can be accepted by the bridgehead nitrogen followed by transport to the protein surface via the proposed proton transfer channel. The only aspect that is

DOI: 10.1021/bi501391d
Biochemistry 2015, 54, 1474−1483

different in the case of HydA1-**1b** is the anchoring of the [2Fe]-subsite with the CN^- ligands in the protein pocket. This could lead to suboptimal stabilization of the [2Fe]-subsite. The lower activity of HydA1-**1b** is probably related to the fact that this H-cluster variant can exist in two isomers: one with a distal CN^- and one with a proximal CN^- ligand. Presumably, only the distal CN^- variant is catalytically active, since here the rotated conformation around the distal iron atom is stabilized by the hydrogen bond of the distal CN^- to Lys_{228}. Furthermore, the reduced negative charge of the [2Fe]-subsite, caused by the missing CN^- ligand, might decrease the catalytic activity of the H-cluster. The CN^- ligand is a powerful σ-donor ligand whereas CO ligands have a strong π-back-bonding effect. The absence of one CN^- ligand and an additional CO ligand likely changes the overall electronic structure of the H-cluster. Presumably, the electron density on the iron center is lowered, which could lead to a less basic amine group.

CONCLUSIONS

A series of modified synthetic binuclear [2Fe]-compounds related to the active center of the native [FeFe]-hydrogenase were introduced into unmaturated HydA1 and tested for their structural and catalytic properties. It was shown that the H_2 production and oxidation activity relies on the same physical and chemical properties of the [2Fe]-subsite. The CN^- ligands establish the overall charge of the [2Fe]-subsite. Apart from this, they do not seem to be essential for the catalytic mechanism. Rather, these CN^- groups stabilize the H-cluster in the protein pocket through electrostatic and hydrogen bonding interactions. Furthermore, the basicity of the azadithiolate moiety is critical for proton binding and transfer into the binding pocket and, therefore, for the catalytic activity of the H-cluster (the propanedithiolate, oxadithiolate, and thiodithiolate variants are strongly reduced in activity). Also, the conformational flexibility (e.g., flipping of the amine group away from Fe_d) and spatial freedom of the azadithiolate moiety plays an important role in the catalytic mechanism. Introduction of steric bulk (*N*-methylazadithiolate bridge) reduces this flexibility and spatial freedom, significantly impairing catalytic activity. Moreover, the protein pocket around the azadithiolate bridge can accommodate substantial steric bulk. This space is, however, probably needed for adaptive conformational changes of the surrounding protein synchronized with those of the binuclear subsite. This may be the reason the dimethyl-azadithiolate variant is not comfortably accommodated in HydA1 and does not show any activity. The H-cluster has sufficient flexibility to allow for alternative but less efficient protonation sites and probably also proton transfer pathways as shown for the case of the propanedithiolate variant.

The novel technique of artificial maturation of [FeFe]-hydrogenases[43,44] introduces many possibilities to engineer semiartificial hydrogenase-derived H_2 producers. However, the introduction of synthetic model compounds into the unmaturated enzyme faces several limitations. First, the protein pocket has defined dimensions and it does not provide space for model compounds of significantly larger size than the native cofactor. On the other hand, small model compounds like mononuclear iron complexes can be easily introduced into the H-cluster pocket, but they seem to have conformations not well tuned to the protein surrounding, which is disadvantageous for catalytic activity. Additionally, the synthetic complex must also be designed in a way that its surface solvation shell is compatible with the cationic protein insertion channel. Preferably, the mimics should be also water-soluble and stable, although alternative maturation conditions could be developed.

So far, most hydrogenase active site model compounds do not fulfill these conditions. A concerted, knowledge based approach addressing both the protein surrounding as well as the inserted binuclear subcluster precursor might provide a road to improved hydrogenases with respect to activity and oxygen sensitivity. The successful insertion of a series of [2Fe]-subsite variants into native unmaturated HydA1 shown in this work demonstrates the viability of such a strategy.

ASSOCIATED CONTENT

Supporting Information

Protein preparation (Figure S1), notes on activity measurements (Figure S2, Table S1), synthesis of $[(NEt_4)_2][Fe_2(pdt)(CO)_4(CN)_2]$ and $[NEt_4][Fe_2(pdt)(CO)_5(CN)]$, stretching modes of $[Fe_2(xdt)(CO)_4(CN)_2]^{2-}$ (Figure S3), stretching modes of HydA1-H_{ox} (Figure S4), stretching modes of $[Fe_2(xdt)(CO)_5(CN)]^-$ (Figure S5), further insertion attempts: mononuclear iron, all-carbonyl and two additional dicyanide compounds (Figure S6), HydA1-**2a**, **3a**, **4**, and **5** (Table S2, Figure S7), HydA1 monocyanide variants (Figure S8, Table S3, Figure S9), HydA1-**6** (Figure S10). This material is available free of charge via the Internet at http://pubs.acs.org.

AUTHOR INFORMATION

Corresponding Authors

*E-mail: edward.reijerse@cec.mpg.de, tel. +49 208 306 3529, fax +49 208 306 3955.

*E-mail: wolfgang.lubitz@cec.mpg.de, tel. +49 208 306 3614, fax +49 208 306 3955.

Funding

This work was supported by the Max-Planck Society and the Deutsche Forschungsgemeinschaft (DIP project LU315/17-1). We also thank the Fonds der Chemischen Industrie for the Doctoral Kekulé Fellowship (K.W.).

Notes

The authors declare no competing financial interest.

ACKNOWLEDGMENTS

We thank Agnes Stoer, Julian Jakobs, Michael Reus, Inge Heise, and Norbert Dickmann for excellent technical assistance. The authors are grateful to Dr. James Birrell for carefully reading the manuscript and his useful suggestions on content and language.

ABBREVIATIONS

adt, azadithiolate; DFT, density functional theory; dime-adt, dimethyl-azadithiolate; DMSO, dimethylsulfoxide; EPR, electron paramagnetic resonance; FTIR, Fourier transform infrared; HydA1-**x**, HydA1 maturated with one of the synthetic mimic variants; odt, oxadithiolate; OHpdt, hydroxo-propanedithiolate; NaDT, sodium dithionite; NMedt, *N*-methylazadithiolate; pdt, propanedithiolate; tdt, thiodithiolate; TEV, tobacco etch virus; THF, tetrahydrofuran; TOF, turnover frequency; Tris, tris(hydroxymethyl)-aminomethane; xdt, one of the dithiolate ligand variants

REFERENCES

(1) Lubitz, W., Ogata, H., Rüdiger, O., and Reijerse, E. (2014) Hydrogenases. *Chem. Rev. 114*, 4081−4148.

DOI: 10.1021/bi501391d
Biochemistry 2015, 54, 1474−1483

(2) Vignais, P. M., and Billoud, B. (2007) Occurrence, classification, and biological function of hydrogenases: an overview. *Chem. Rev. 107*, 4206−4272.
(3) Kubas, G. J. (2007) Fundamentals of H_2 binding and reactivity on transition metals underlying hydrogenase function and H_2 production and storage. *Chem. Rev. 107*, 4152−4205.
(4) Adams, M. W. W. (1990) The structure and mechanism of iron-hydrogenases. *Biochim. Biophys. Acta: Bioenerg. 1020*, 115−145.
(5) Hatchikian, E. C., Forget, N., Fernandez, V. M., Williams, R., and Cammack, R. (1992) Further characterization of the [Fe]-hydrogenase from *Desulfovibrio desulfuricans* ATCC 7757. *Eur. J. Biochem. 209*, 357−365.
(6) Happe, T., and Naber, J. D. (1993) Isolation, characterization and N-terminal amino acid sequence of hydrogenase from the green alga *Chlamydomonas reinhardtii*. *Eur. J. Biochem. 214*, 475−481.
(7) Nicolet, Y., Piras, C., Legrand, P., Hatchikian, C. E., and Fontecilla-Camps, J. C. (1999) *Desulfovibrio desulfuricans* iron hydrogenase: the structure shows unusual coordination to an active site Fe binuclear center. *Structure 7*, 13−23.
(8) Peters, J. W., Lanzilotta, W. N., Lemon, B. J., and Seefeldt, L. C. (1998) X-ray crystal structure of the Fe-only hydrogenase (CpI) from *Clostridium pasteurianum* to 1.8 angstrom resolution. *Science 282*, 1853−1858.
(9) Volbeda, A., Garcin, E., Piras, C., de Lacey, A. L., Fernandez, V. M., Hatchikian, E. C., Frey, M., and Fontecilla-Camps, J. C. (1996) Structure of the [NiFe] hydrogenase active site: evidence for biologically uncommon Fe ligands. *J. Am. Chem. Soc. 118*, 12989−12996.
(10) Vignais, P. M., Billoud, B., and Meyer, J. (2001) Classification and phylogeny of hydrogenases1. *FEMS Microbiol. Rev. 25*, 455−501.
(11) Frey, M. (2002) Hydrogenases: hydrogen-activating enzymes. *ChemBioChem 3*, 153−160.
(12) Artero, V., and Fontecave, M. (2005) Some general principles for designing electrocatalysts with hydrogenase activity. *Coord. Chem. Rev. 249*, 1518−1535.
(13) Wang, M., Chen, L., and Sun, L. (2012) Recent progress in electrochemical hydrogen production with earth-abundant metal complexes as catalysts. *Energy Environ. Sci. 5*, 6763−6778.
(14) Darensbourg, M. Y., Lyon, E. J., and Smee, J. J. (2000) The bio-organometallic chemistry of active site iron in hydrogenases. *Coord. Chem. Rev. 206−207*, 533−561.
(15) Gloaguen, F., and Rauchfuss, T. B. (2009) Small molecule mimics of hydrogenases: hydrides and redox. *Chem. Soc. Rev. 38*, 100−108.
(16) Tard, C., and Pickett, C. J. (2009) Structural and functional analogues of the active sites of the [Fe]-, [NiFe]-, and [FeFe]-hydrogenases. *Chem. Rev. 109*, 2245−2274.
(17) Sun, L., Åkermark, B., and Ott, S. (2005) Iron hydrogenase active site mimics in supramolecular systems aiming for light-driven hydrogen production. *Coord. Chem. Rev. 249*, 1653−1663.
(18) Simmons, T. R., Berggren, G., Bacchi, M., Fontecave, M., and Artero, V. (2014) Mimicking hydrogenases: From biomimetics to artificial enzymes. *Coord. Chem. Rev. 270−271*, 127−150.
(19) Nicolet, Y., de Lacey, A. L., Vernède, X., Fernandez, V. M., Hatchikian, E. C., and Fontecilla-Camps, J. C. (2001) Crystallographic and FTIR spectroscopic evidence of changes in Fe coordination upon reduction of the active site of the Fe-only hydrogenase from *Desulfovibrio desulfuricans*. *J. Am. Chem. Soc. 123*, 1596−1601.
(20) Happe, T., and Kaminski, A. (2002) Differential regulation of the Fe-hydrogenase during anaerobic adaptation in the green alga *Chlamydomonas reinhardtii*. *Eur. J. Biochem. 269*, 1022−1032.
(21) Posewitz, M. C., King, P. W., Smolinski, S. L., Zhang, L., Seibert, M., and Ghirardi, M. L. (2004) Discovery of two novel radical s-adenosylmethionine proteins required for the assembly of an active [Fe] hydrogenase. *J. Biol. Chem. 279*, 25711−25720.
(22) Shepard, E. M., Mus, F., Betz, J. N., Byer, A. S., Duffus, B. R., Peters, J. W., and Broderick, J. B. (2014) [FeFe]-hydrogenase maturation. *Biochemistry 53*, 4090−4104.
(23) Kuchenreuther, J. M., Myers, W. K., Stich, T. A., George, S. J., NejatyJahromy, Y., Swartz, J. R., and Britt, R. D. (2013) A radical intermediate in tyrosine scission to the CO and CN^- ligands of FeFe hydrogenase. *Science 342*, 472−475.
(24) Kuchenreuther, J. M., Myers, W. K., Suess, D. L. M., Stich, T. A., Pelmenschikov, V., Shiigi, S. A., Cramer, S. P., Swartz, J. R., Britt, R. D., and George, S. J. (2014) The HydG enzyme generates an $Fe(CO)_2(CN)$ synthon in assembly of the FeFe hydrogenase H-cluster. *Science 343*, 424−427.
(25) Lemon, B. J., and Peters, J. W. (1999) Binding of exogenously added carbon monoxide at the active site of the iron-only hydrogenase (CpI) from *Clostridium pasteurianum*. *Biochemistry 38*, 12969−12973.
(26) Silakov, A., Kamp, C., Reijerse, E., Happe, T., and Lubitz, W. (2009) Spectroelectrochemical characterization of the active site of the [FeFe] hydrogenase HydA1 from *Chlamydomonas reinhardtii*. *Biochemistry 48*, 7780−7786.
(27) Fontecilla-Camps, J. C., Amara, P., Cavazza, C., Nicolet, Y., and Volbeda, A. (2009) Structure−function relationships of anaerobic gas-processing metalloenzymes. *Nature 460*, 814−822.
(28) Fontecilla-Camps, J. C., Volbeda, A., Cavazza, C., and Nicolet, Y. (2007) Structure/function relationships of [NiFe]- and [FeFe]-hydrogenases. *Chem. Rev. 107*, 4273−4303.
(29) Lubitz, W., Reijerse, E., and van Gastel, M. (2007) [NiFe] and [FeFe] hydrogenases studied by advanced magnetic resonance techniques. *Chem. Rev. 107*, 4331−4365.
(30) Pierik, A. J., Hulstein, M., Hagen, W. R., and Albracht, S. P. J. (1998) A low-spin iron with CN and CO as intrinsic ligands forms the core of the active site in [Fe]-hydrogenases. *Eur. J. Biochem. 258*, 572−578.
(31) Mulder, D. W., Boyd, E. S., Sarma, R., Lange, R. K., Endrizzi, J. A., Broderick, J. B., and Peters, J. W. (2010) Stepwise [FeFe]-hydrogenase H-cluster assembly revealed in the structure of $HydA^{\Delta EFG}$. *Nature 465*, 248−251.
(32) Pandey, A. S., Harris, T. V., Giles, L. J., Peters, J. W., and Szilagyi, R. K. (2008) Dithiomethylether as a ligand in the hydrogenase H-cluster. *J. Am. Chem. Soc. 130*, 4533−4540.
(33) Schrodinger, L. (2010) The PyMOL Molecular Graphics System, version 1.3r1.
(34) Volbeda, A., Charon, M.-H., Piras, C., Hatchikian, E. C., Frey, M., and Fontecilla-Camps, J. C. (1995) Crystal structure of the nickel-iron hydrogenase from *Desulfovibrio gigas*. *Nature 373*, 580−587.
(35) Montet, Y., Amara, P., Volbeda, A., Vernède, X., Hatchikian, E. C., Field, M. J., Frey, M., and Fontecilla-Camps, J. C. (1997) Gas access to the active site of Ni-Fe hydrogenases probed by X-ray crystallography and molecular dynamics. *Nat. Struct. Mol. Biol. 4*, 523−526.
(36) Le Cloirec, A., C. Davies, S., J. Evans, D., L. Hughes, D., J. Pickett, C., P. Best, S., and Borg, S. (1999) A di-iron dithiolate possessing structural elements of the carbonyl/cyanide sub-site of the H-centre of Fe-only hydrogenase. *Chem. Commun.*, 2285−2286.
(37) Lyon, E. J., Georgakaki, I. P., Reibenspies, J. H., and Darensbourg, M. Y. (1999) Carbon monoxide and cyanide ligands in a classical organometallic complex model for Fe-only hydrogenase. *Angew. Chem., Int. Ed. 38*, 3178−3180.
(38) Schmidt, M., Contakes, S. M., and Rauchfuss, T. B. (1999) First generation analogues of the binuclear site in the Fe-only hydrogenases: $Fe_2(\mu\text{-}SR)_2(CO)_4(CN)_2^{2-}$. *J. Am. Chem. Soc. 121*, 9736−9737.
(39) Li, H., and Rauchfuss, T. B. (2002) Iron carbonyl sulfides, formaldehyde, and amines condense to give the proposed azadithiolate cofactor of the Fe-only hydrogenases. *J. Am. Chem. Soc. 124*, 726−727.
(40) Song, L.-C., Yang, Z.-Y., Bian, H.-Z., and Hu, Q.-M. (2004) Novel single and double diiron oxadithiolates as models for the active site of [Fe]-only hydrogenases. *Organometallics 23*, 3082−3084.
(41) Silakov, A., Wenk, B., Reijerse, E., and Lubitz, W. (2009) ^{14}N HYSCORE investigation of the H-cluster of [FeFe] hydrogenase: evidence for a nitrogen in the dithiol bridge. *Phys. Chem. Chem. Phys. 11*, 6592−6599.
(42) Erdem, Ö. F., Schwartz, L., Stein, M., Silakov, A., Kaur-Ghumaan, S., Huang, P., Ott, S., Reijerse, E. J., and Lubitz, W. (2011)

DOI: 10.1021/bi501391d
Biochemistry 2015, 54, 1474−1483

A model of the [FeFe] hydrogenase active site with a biologically relevant azadithiolate bridge: a spectroscopic and theoretical investigation. *Angew. Chem., Int. Ed. 50*, 1439−1443.
(43) Berggren, G., Adamska, A., Lambertz, C., Simmons, T. R., Esselborn, J., Atta, M., Gambarelli, S., Mouesca, J. M., Reijerse, E., Lubitz, W., Happe, T., Artero, V., and Fontecave, M. (2013) Biomimetic assembly and activation of FeFe-hydrogenases. *Nature 499*, 66−70.
(44) Esselborn, J., Lambertz, C., Adamska-Venkatesh, A., Simmons, T., Berggren, G., Noth, J., Siebel, J., Hemschemeier, A., Artero, V., Reijerse, E., Fontecave, M., Lubitz, W., and Happe, T. (2013) Spontaneous activation of [FeFe]-hydrogenases by an inorganic [2Fe] active site mimic. *Nat. Chem. Biol. 9*, 607−609.
(45) Adamska-Venkatesh, A., Krawietz, D., Siebel, J., Weber, K., Happe, T., Reijerse, E., and Lubitz, W. (2014) New redox states observed in [FeFe] hydrogenases reveal redox coupling within the H-cluster. *J. Am. Chem. Soc. 136*, 11339−11346.
(46) Akhtar, M., and Jones, P. (2008) Deletion of *isc*R stimulates recombinant clostridial Fe−Fe hydrogenase activity and H_2-accumulation in *Escherichia coli* BL21(DE3). *Appl. Microbiol. Biotechnol. 78*, 853−862.
(47) Kuchenreuther, J. M., Grady-Smith, C. S., Bingham, A. S., George, S. J., Cramer, S. P., and Swartz, J. R. (2010) High-yield expression of heterologous [FeFe] hydrogenases in *Escherichia coli*. *ONE 5*, e15491.
(48) Winkler, M., Hemschemeier, A., Gotor, C., Melis, A., and Happe, T. (2002) [Fe]-hydrogenases in green algae: photo-fermentation and hydrogen evolution under sulfur deprivation. *Int. J. Hydrogen Energy 27*, 1431−1439.
(49) Fish, W. W. (1988) Rapid colorimetric micromethod for the quantitation of complexed iron in biological samples. *Methods Enzymol. 158*, 357−364.
(50) Winter, A., Zsolnai, L., and Huttner, G. (1982) Dinuclear and trinuclear carbonlyairon complexes containing 1,2-dithiolato bridging ligands. *Z. Naturforsch., B: Chem. Sci. 37*, 1430−1436.
(51) Stanley, J. L., Heiden, Z. M., Rauchfuss, T. B., Wilson, S. R., De Gioia, L., and Zampella, G. (2007) Desymmetrized diiron azadithiolato carbonyls: a step toward modeling the iron-only hydrogenases. *Organometallics 27*, 119−125.
(52) Song, L.-C., Yang, Z.-Y., Hua, Y.-J., Wang, H.-T., Liu, Y., and Hu, Q.-M. (2007) Diiron thiadithiolates as active site models for the iron-only hydrogenases: synthesis, structures, and catalytic H_2 production. *Organometallics 26*, 2106−2110.
(53) Song, L.-C., Li, C.-G., Gao, J., Yin, B.-S., Luo, X., Zhang, X.-G., Bao, H.-L., and Hu, Q.-M. (2008) Synthesis, structure, and electrocatalysis of diiron C-functionalized propanedithiolate (PDT) complexes related to the active site of [FeFe]-hydrogenases. *Inorg. Chem. 47*, 4545−4553.
(54) King, R. B. (1962) Organosulfur derivatives of metal carbonyls. I. The isolation of two isomeric products in the reaction of triiron dodecacarbonyl with dimethyl disulfide. *J. Am. Chem. Soc. 84*, 2460−2460.
(55) Gloaguen, F., Lawrence, J. D., Schmidt, M., Wilson, S. R., and Rauchfuss, T. B. (2001) Synthetic and structural studies on $[Fe_2(SR)_2(CN)_x(CO)_{6-x}]^{x-}$ as active site models for Fe-only hydrogenases. *J. Am. Chem. Soc. 123*, 12518−12527.
(56) Kayal, A., and Rauchfuss, T. B. (2003) Protonation studies of the new iron carbonyl cyanide trans-$[Fe(CO)_3(CN)_2]^{2-}$: implications with respect to hydrogenases. *Inorg. Chem. 42*, 5046−5048.
(57) Rauchfuss, T. B., Contakes, S. M., Hsu, S. C. N., Reynolds, M. A., and Wilson, S. R. (2001) The influence of cyanide on the carbonylation of iron(II): synthesis of Fe−SR−CN−CO centers related to the hydrogenase active sites. *J. Am. Chem. Soc. 123*, 6933−6934.
(58) Mulder, D. W., Shepard, E. M., Meuser, J. E., Joshi, N., King, P. W., Posewitz, M. C., Broderick, J. B., and Peters, J. W. (2011) Insights into [FeFe]-hydrogenase structure, mechanism, and maturation. *Structure 19*, 1038−1052.
(59) Finkelmann, A. R., Stiebritz, M. T., and Reiher, M. (2014) Inaccessibility of the μ-hydride species in [FeFe] hydrogenases. *Chem. Sci. 5*, 215−221.
(60) Knörzer, P., Silakov, A., Foster, C. E., Armstrong, F. A., Lubitz, W., and Happe, T. (2012) Importance of the protein framework for catalytic activity of [FeFe]-hydrogenases. *J. Biol. Chem. 287*, 1489−1499.
(61) Greco, C., Bruschi, M., Heimdal, J., Fantucci, P., De Gioia, L., and Ryde, U. (2007) Structural insights into the active-ready form of [FeFe]-hydrogenase and mechanistic details of its inhibition by carbon monoxide. *Inorg. Chem. 46*, 7256−7258.
(62) Yu, L., Greco, C., Bruschi, M., Ryde, U., De Gioia, L., and Reiheet, M. (2011) Targeting intermediates of FeFe-hydrogenase by CO and CN vibrational signatures. *Inorg. Chem. 50*, 3888−3900.
(63) Roseboom, W., de Lacey, A. L., Fernandez, V. M., Hatchikian, E. C., and Albracht, S. P. J. (2006) The active site of the [FeFe]-hydrogenase from *Desulfovibrio desulfuricans*. II. Redox properties, light sensitivity and CO-ligand exchange as observed by infrared spectroscopy. *J. Biol. Inorg. Chem. 11*, 102−118.
(64) Adamska, A., Silakov, A., Lambertz, C., Rüdiger, O., Happe, T., Reijerse, E., and Lubitz, W. (2012) Identification and characterization of the "super-reduced" state of the H-cluster in [FeFe] hydrogenase: a new building block for the catalytic cycle? *Angew. Chem., Int. Ed. 51*, 11458−11462.
(65) Zhou, T. J., Mo, Y. R., Liu, A. M., Zhou, Z. H., and Tsai, K. R. (2004) Enzymatic mechanism of Fe-only hydrogenase: Density functional study on H-H making/breaking at the diiron cluster with concerted proton and electron transfers. *Inorg. Chem. 43*, 923−930.
(66) Bruschi, M., Fantucci, P., and De Gioia, L. (2002) DFT investigation of structural, electronic, and catalytic properties of diiron complexes related to the $[2Fe]_H$ subcluster of Fe-only hydrogenases. *Inorg. Chem. 41*, 1421−1429.
(67) Bruschi, M., Fantucci, P., and De Gioia, L. (2003) Density functional theory investigation of the active site of [Fe]-hydrogenases: effects of redox state and ligand characteristics on structural, electronic, and reactivity properties of complexes related to the $[2Fe]_H$ subcluster. *Inorg. Chem. 42*, 4773−4781.

DOI: 10.1021/bi501391d
Biochemistry 2015, 54, 1474−1483